Backscattering Effects on High-Speed Modulation of Strongly Injection-Locked Whistle-Geometry Semiconductor Ring Lasers

Gennady A. Smolyakov and Marek Osiński, *Life Fellow, IEEE*

***Abstract*—An injection-locking scheme, involving a single-frequency master laser monolithically integrated with a unidirectional whistle-geometry semiconductor microring laser, has been proposed for enhanced ultra-high-speed performance. Greatly enhanced high-speed modulation performance of the strong-injection-locking scheme has been predicted in numerical calculations. In our previous analysis, however, linear coupling between the two counter-propagating modes due to light backscattering was not taken into account. In this work, we investigate the potential negative impact of light backscattering between the two counter-propagating modes on high-speed modulation performance of strongly injection-locked unidirectional whistle-geometry semiconductor microring lasers.**

***Index Terms*—Direct modulation, light backscattering, modulation response, monolithic integration, optical injection locking, semiconductor ring lasers.**

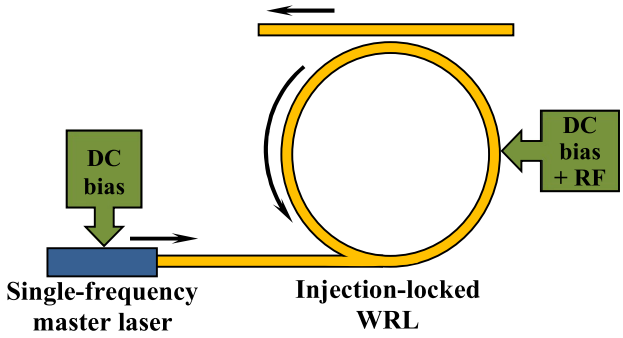

Fig. 1. Schematic diagram of a strongly optically injection-locked whistle-geometry semiconductor ring laser monolithically integrated with a single-frequency master laser. The injecting waveguide is maintained at transparency.

I. Introduction

OPTICAL injection locking is a well-established technique to improve ultrahigh frequency performance of semiconductor lasers and to reach beyond the record values of modulation bandwidth achieved in free-running devices [1]. Enhanced microwave performance has been reported in edge-emitting lasers with Fabry-Perot cavity [2]–[4], DFB lasers [5]–[8], and VCSELs [8]–[17]. The highest 3-dB modulation bandwidth of ∼80 GHz observed so far in injection-locked VCSELs and DFB lasers [8] by far exceeds modulation bandwidths achieved in free-running devices. In 2020, Chorchos and co-workers demonstrated the NRZ (non-return-to-zero) data transmission carried by an 850-nm VCSEL at 80 Gbit/s over 2-m multimode fiber and 72 Gbit/s over 50-m multimode fiber [18].

Subjecting a semiconductor laser to strong optical injection is key to reaching the ultimate limits of modulation bandwidth enhancement. The coupling rate coefficient κ_c for optical injection locking is:

$$\kappa_c = c\sqrt{1-R}/\left(2n_{\text{eff}}L\right) = \sqrt{1-R}/\tau_{\text{rt}}, \qquad (1)$$

where R is the reflectivity of the laser mirror through which the light is injected, L is the slave laser cavity length, c is the speed of light in vacuum, n_{eff} is the modal effective index, and $\tau_{\text{rt}} = 2n_{\text{eff}}L/c$ is the cavity roundtrip time. To maximize the injection coupling rate coefficient κ_c, the smallest possible values for both τ_{rt} and R are desirable in injection-locked lasers. Optimization of both edge-emitting laser and VCSEL designs for enhanced high-speed performance inherently involves a trade-off between these two parameters, as dictated by the requirement to keep threshold current at an acceptable level. Further improvement of modulation bandwidth in injection-locked VCSELs can come solely from increasing the power of master lasers used for optical injection. The data rate of the NRZ transmission can hardly achieve 100 Gbit/s, so setting several VCSEL chips as the VCSEL array to aggregate the whole data rate was mentioned in [19] as the only method to achieve the data rates of the NRZ transmission beyond that level. Special complex data formats, such as 4-level pulse amplitude modulation (PAM-4) or quadrature amplitude modulation orthogonal frequency division multiplexing (QAM-OFDM), are necessary to maximize the encoding data rate under the same modulation bandwidth of solitary VCSELs [19].

To overcome these limitations of VCSELs and Fabry-Perot lasers, we have proposed a strong-injection-locking scheme of a single-frequency master laser monolithically integrated with a unidirectional whistle-geometry microring laser (WRL) [20], [21]. The structure of WRL shown schematically in Fig. 1 strongly favors the counterclockwise (CCW) mode over the

Manuscript received 17 July 2022; revised 3 August 2022; accepted 5 August 2022. Date of publication 9 August 2022; date of current version 25 August 2022. This work was supported by the Office of Naval Research under Grants N00014-17-1-2416 and N00014-21-1-2683. *(Corresponding author: Marek Osiński.)*

The authors are with the Center for High Technology Materials, University of New Mexico, Albuquerque, NM 87106-4343 USA (e-mail: gen@chtm.unm.edu; osinski@chtm.unm.edu).

Digital Object Identifier 10.1109/JPHOT.2022.3197520

clockwise (CW) mode, even in absence of any injected light. The unidirectionality of the whistle-geometry configuration has been confirmed through rigorous three-dimensional finite-difference time-domain (FDTD) simulation by showing a strong asymmetry in propagation losses and, therefore, in photon lifetimes between the two counterpropagating modes [22]. The WRL scheme allows for strong coupling of the master laser output into the ring laser, thus providing dramatically increased injection coupling rate as compared with the traditional optical injection scheme based on a waveguide directional coupler adjacent to the ring laser [23]. An additional advantage of the WRL design is that it allows for tuning of the master laser wavelength without affecting the coupling efficiency into the ring, which is not the case when a directional coupler is used. We predicted greatly enhanced resonance frequency of up to ∼160 GHz in numerical calculations for the strongly injection-locked WRL [21]. In our previous analysis, however, linear coupling between the two counterpropagating modes due to light backscattering was not taken into account. Light backscattering in semiconductor ring lasers, designed as unidirectional, can result in directional bistability or even bidirectional operation, with the power in the two counterpropagating modes being roughly equal [24], [25]. The potential negative impact of light backscattering between the two counterpropagating modes on high-speed modulation performance of strongly injection-locked unidirectional WRLs is the subject of this paper.

II. Theoretical Model

To model dynamics of an optically injection-locked microring laser monolithically integrated with a single-frequency master laser, a system of rate equations was previously used, written in terms of the photon numbers, phases, and total carrier numbers in the master laser and the microring slave laser, respectively [20], [21], [23]. Here, the model presented in [20], [21] for strong optical injection locking of a WRL monolithically integrated with a single-frequency master laser (Fig. 1) is extended by taking into account light backscattering, causing a linear coupling between the two counterpropagating modes:

$$\frac{dS_m}{dt} = \left[G_{0m}\left(N_m - N_{0m}\right) - \frac{1}{\tau_{\mathrm{p}}^{\mathrm{m}}}\right] S_m + R_{sp} \quad (2)$$

$$\frac{d\theta_{\mathrm{m}}}{dt} = \frac{\alpha}{2}\left[G_{0m}\left(N_m - N_{0m}\right) - \frac{1}{\tau_{\mathrm{p}}^{\mathrm{m}}}\right] \quad (3)$$

$$\frac{dN_m}{dt} = \eta_i \frac{I_m}{q} - \frac{N_m}{\tau_{\mathrm{c}}} - G_{0m}\left(N_m - N_{0m}\right) S_m \quad (4)$$

$$\begin{aligned}\frac{dS_{ccw}}{dt} &= \left[G_{ccw} - \frac{1}{\tau_{\mathrm{p}}^{\mathrm{ccw}}}\right] S_{ccw} + R_{sp} \\ &\quad + 2\kappa_{\mathrm{c}}\sqrt{S_m S_{ccw}}\, cos\left(\theta_{\mathrm{ccw}} - \theta_{\mathrm{m}}\right) \\ &\quad + 2\kappa_{\mathrm{s}}\sqrt{S_{cw} S_{ccw}}\, cos\left(\theta_{\mathrm{ccw}} - \theta_{\mathrm{cw}} - \theta_{\mathrm{s}}\right) \quad (5)\end{aligned}$$

$$\begin{aligned}\frac{d\theta_{\mathrm{ccw}}}{dt} &= \frac{\alpha}{2}\left[G_{ccw} - \frac{1}{\tau_{\mathrm{p}}^{\mathrm{ccw}}}\right] - \left(\omega_0 - \omega_{\mathrm{th}}\right) \\ &\quad - \kappa_{\mathrm{c}}\sqrt{\frac{S_m}{S_{ccw}}}\, sin\left(\theta_{\mathrm{ccw}} - \theta_{\mathrm{m}}\right) \\ &\quad - \kappa_{\mathrm{s}}\sqrt{\frac{S_{cw}}{S_{ccw}}}\, sin\left(\theta_{\mathrm{ccw}} - \theta_{\mathrm{cw}} - \theta_{\mathrm{s}}\right) \quad (6)\end{aligned}$$

$$\begin{aligned}\frac{dS_{cw}}{dt} &= \left[G_{cw} - \frac{1}{\tau_{\mathrm{p}}^{\mathrm{cw}}}\right] S_{cw} + R_{sp} \\ &\quad + 2\kappa_{\mathrm{s}}\sqrt{S_{ccw} S_{cw}}\, cos\left(\theta_{\mathrm{cw}} - \theta_{\mathrm{ccw}} - \theta_{\mathrm{s}}\right) \quad (7)\end{aligned}$$

$$\begin{aligned}\frac{d\theta_{\mathrm{cw}}}{dt} &= \frac{\alpha}{2}\left[G_{cw} - \frac{1}{\tau_{p}^{\mathrm{cw}}}\right] - \left(\omega_0 - \omega_{\mathrm{th}}\right) \\ &\quad - \kappa_{\mathrm{s}}\sqrt{\frac{S_{ccw}}{S_{cw}}}\, sin\left(\theta_{\mathrm{cw}} - \theta_{\mathrm{ccw}} - \theta_{\mathrm{s}}\right) \quad (8)\end{aligned}$$

$$\frac{dN_r}{dt} = \eta_i \frac{I_r}{q} - \frac{N_r}{\tau_{\mathrm{c}}} - G_{cw} S_{cw} - G_{ccw} S_{ccw} \quad (9)$$

In (2)–(4), the photon number S_{m} and the optical phase θ_{m} are related to the normalized complex field envelope E_{m} of the master laser as $E_m = \sqrt{S_m}\exp(i\theta_m(t))$. N_{m} represents the total carrier number in the master laser, and we assume uniform carrier density in the laser cavity. The differential modal gain $G_{0\mathrm{m}}$ is given by

$$G_{0m} = \frac{\Gamma a v_g}{V_m}, \quad (10)$$

where Γ is the optical confinement factor, a is the differential gain, v_{g} is the group velocity, and V_{m} is the volume of the active region of the master laser. Other parameters in (2)–(4) are the transparency carrier number $N_{0\mathrm{m}}$, the photon lifetime $\tau_{\mathrm{p}}^{\mathrm{m}}$, the spontaneous emission rate R_{sp}, the linewidth broadening factor α, the bias current I_{m}, the internal quantum efficiency η_{i}, the electron charge q, and the carrier lifetime τ_{c}.

We model the ring laser in (5)–(9) by two counter-propagating modes with the photon numbers $\mathcal{S}_{\mathrm{cw}}, \mathcal{S}_{\mathrm{ccw}}$ and optical phases θ_{cw}, θ_{ccw} for the clockwise (CW) and counterclockwise (CCW) modes, respectively. The master laser light is injected into the CCW mode. The total carrier number in the ring laser is described by N_{r}, and we assume uniform carrier density in the ring laser cavity. Unequal photon lifetimes $\tau_{\mathrm{p}}^{\mathrm{cw}}$ and $\tau_{\mathrm{p}}^{\mathrm{ccw}}$ are allowed in the model for the CW and CCW modes, respectively, accounting for the asymmetric design of the WRL cavity. Nonlinear gain saturation effects are represented in (5)–(9) by coefficients ε_{s} and ε_{c} for the self- and cross-gain saturation in the expressions for the modal gain, with $\varepsilon_{\mathrm{c}} = 2\varepsilon_{\mathrm{s}}$ [26]:

$$\begin{aligned}G_{cw} &= \frac{G_{0r}\left(N_r - N_{0r}\right)}{1 + \varepsilon_{\mathrm{s}} S_{cw}/V_r + \varepsilon_{\mathrm{c}} S_{ccw}/V_r} \\ G_{ccw} &= \frac{G_{0r}\left(N_r - N_{0r}\right)}{1 + \varepsilon_{\mathrm{s}} S_{ccw}/V_r + \varepsilon_{\mathrm{c}} S_{cw}/V_r}\end{aligned} \quad (11)$$

where $N_{0\mathrm{r}}$ is the transparency carrier number, and the differential modal gain $G_{0\mathrm{r}}$ is given by

$$G_{0r} = \frac{\Gamma a v_g}{V_r}. \quad (12)$$

V_{r} in (12) is the volume of the active region of the ring laser. Other parameters in (5)–(9) are the injection coupling rate κ_{c},

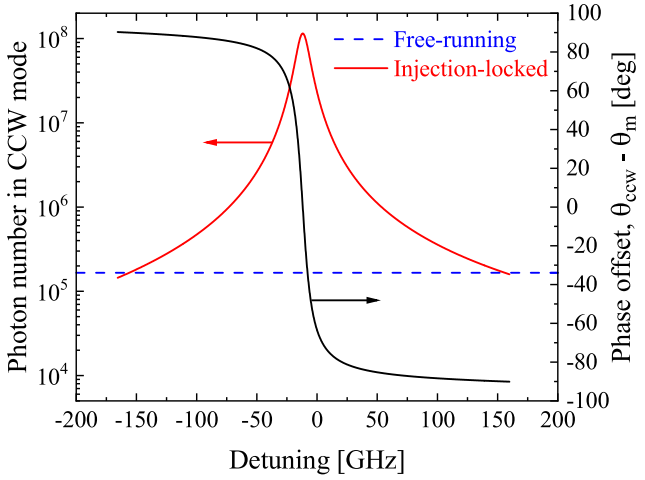

Fig. 2. Photon number in the CCW mode of the injection-locked WRL (red curve) and optical phase offset between the master laser and the CCW mode of the injection-locked WRL (black curve) versus frequency detuning under steady-state conditions. $I_{\rm m} = 12$ mA, $I_{\rm r} = 6$ mA [21].

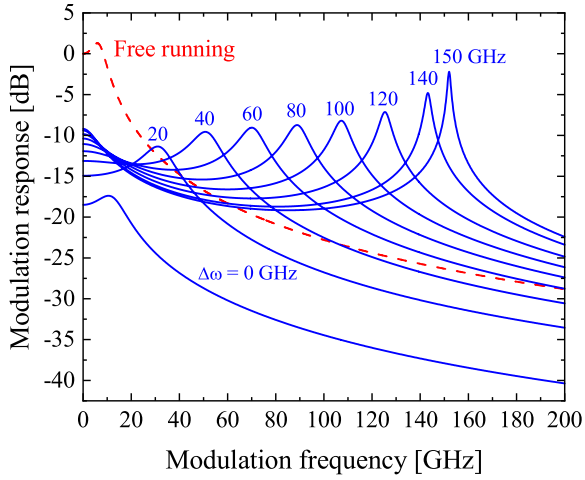

Fig. 3. Modulation frequency response of the free-running WRL (red dashed curve) and that of the strongly injection-locked WRL (blue solid curves) calculated for several values of positive frequency detuning. Modulation frequency response is normalized to low-frequency response of the free-running WRL. $I_{\rm m} = 12$ mA, $I_{\rm r} = 6$ mA [21].

the free-running mode frequency of the ring cavity ω_0, and the free-running mode frequency of the ring cavity at threshold $\omega_{\rm th}$. In the analysis of free-running ring laser operation, we set ω_0 - $\omega_{\rm th}$ equal to zero in (6) and (8), thus neglecting the drift of the resonant cavity frequency above threshold. Under stable injection-locking conditions, ω_0 in (6) is locked to the frequency of the master laser, and ω_0 in (8) is locked to the frequency of the predominant CCW mode of the ring laser due to light backscattering. The term ω_0 - $\omega_{\rm th}$ in (6) and (8), therefore, represents effectively the angular frequency detuning between the master laser and the ring laser.

Linear coupling between the two counterpropagating modes due to light backscattering is taken into account through the coupling rate $\kappa_{\rm s}\exp(i\theta_{\rm s})$. In the following analysis, we set $\theta_{\rm s}$ equal to zero and assume the coupling rate due to light backscattering to be a real number. The backscattering coefficient $\kappa_{\rm s}$ is further discussed in Section III.

All mechanisms that could possibly lead to feedback from the ring laser to the master laser are neglected in the modelling. Thus, we assume zero reflection from the interface between the injecting waveguide and the ring laser. In the WRL injection-locking scheme, the ring laser unidirectionality is imposed by optical injection locking and further promoted by the strong asymmetry in optical losses between the CW and CCW modes. Therefore, there is no stimulated emission from the CW mode of the ring laser that might reach the master laser. Any optical feedback to the master laser resulting from light backscattering or from the CW mode spontaneous emission is also neglected.

In practice, if needed, the condition of no optical feedback to the master laser could either be realized by inserting on-chip optical isolators [27], or by implementing tapered loss outcoupling waveguides illustrated in Figs. 2 and 3 of [28].

Parameters used in the simulation are shown in Table I. Specifics of a single-transverse-mode 1.55-μm GaInAs/AlGaInAs/InP MQW deeply etched ridge-waveguide laser structure, assumed in the simulation, as well as details on how the parameters were determined can be found in [20], [21].

III. Numerical Simulations

We carried out simulations for the same configuration and under the same bias conditions that were assumed in [20], [21] for the master and the ring lasers. Throughout the simulations, master laser bias of 12 mA (corresponding to 2 times the threshold current $I_{\rm th,m}$) and ring laser bias of 6 mA (corresponding to 3 times the threshold current $I_{\rm th,r}$) were consistently chosen. The results of steady-state and modulation analysis presented in [20], [21] correspond to the strongly injection-locked WRL with no backscattering in the ring laser and can be used, therefore, as a starting point for the present analysis. One of the most important findings in [20], [21] was that the high injection coupling rate in WRL configuration leads to a very wide range of stable injection locking of the ring laser. The ring laser remains stably locked for the frequency detuning $\Delta\omega$ between -165 GHz and 160 GHz (Fig. 2).

The modulation frequency response of the strongly injection-locked WRL calculated for several positive values of frequency detuning is shown in Fig. 3. Also shown is the free-running WRL modulation response, characterized by the 3-dB modulation bandwidth of ~11.5 GHz and the resonance frequency of ~5.9 GHz. As can be seen, great enhancement (up to ~150 GHz) in the resonance frequency of the injection-locked WRL is achieved as the frequency detuning approaches the edges of the stable locking range. The phase offset changes from zero (the strongest locking condition) in the middle of the stable injection-locking range to $\pi/2$ or $-\pi/2$ at the boundaries of the stable injection-locking range (the weakest locking condition). Outside that range of frequency detuning the locking is lost.

We consider a single backscattering event over the cavity roundtrip. In this case, the coupling coefficient due to backscattering $\kappa_{\rm s}$ is related to the amplitude backscattering coefficient S

TABLE I
PARAMETERS USED IN SIMULATION

Parameters	Symbol	Value	Units
Material and structural parameters			
Linewidth broadening factor	α	2	
Carrier lifetime	τ_c	0.4	ns
Spontaneous emission rate	R_{sp}	85	ns^{-1}
Differential gain	a	1×10^{-15}	cm^2
Transparency carrier density	N_0/V	$\sim0.485\times10^{18}$	cm^{-3}
Internal quantum efficiency	η_i	0.5	
Optical confinement factor	Γ	0.09	
Modal effective index	n_{eff}	3.279	
Group velocity	v_g	8.76×10^9	cm/s
Master laser			
Cavity length	L_m	200	μm
Reflectivity of injecting mirror	R_m	0.825	
Active region volume	V_m	1.372×10^{-11}	cm^3
Transparency carrier number	N_{0m}	6.65×10^6	
Photon lifetime	τ_p^m	22.74	ps
Ring laser			
Injection coupling rate	κ_c	6.09×10^{11}	s^{-1}
Ring diameter	d	20	μm
Effective cavity length	L_r	62.83	μm
Active region volume	V_r	4.31×10^{-12}	cm^3
Transparency carrier number	N_{0r}	2.089×10^6	
Photon lifetime in CCW mode	τ_p^{ccw}	13.4	ps
Photon lifetime in CW mode	τ_p^{cw}	0.69	ps
Nonlinear gain self-saturation	ε_s	2.7×10^{-18}	cm^3
Nonlinear gain cross-saturation	ε_c	5.4×10^{-18}	cm^3

as follows:

$$\kappa_s = \frac{cS}{\pi n_{eff} d}, \tag{13}$$

where c and n_{eff} have been defined in Section I, and d is the ring laser diameter. The calculated dependence of κ_s versus S for the WRL parameters specified in Table I is given in Fig. 4, where the red dashed line corresponding to the value of injection coupling rate κ_c is shown for comparison. In this paper, we present the results of our analysis as a function of the backscattering coefficient S.

The detuning between the frequency of injected light and that of the cavity mode is known to control the enhanced resonance frequency in the modulation response of injection-locked semiconductor lasers. In this paper, we show the results for several values of positive frequency detuning $\Delta\omega$ of interest ($\Delta\omega = 50$ GHz, 80 GHz, 120 GHz, and 150 GHz), keeping in mind that approaching the boundary of the stable locking range corresponds to progressively weaker locking conditions (see Fig. 2). The results obtained for negative frequency detuning are very similar to those shown here for positive frequency detuning.

We first consider the case of a relatively strong injection locking, with $\Delta\omega = 50$ GHz. For S exceeding 3×10^{-6}, the CW mode gets locked by the CCW mode, leading to stable intensity output (Fig. 5). Further increase in S results in weakening and eventual loss of injection locking between the master laser and the CCW mode of the ring laser at $S = 0.03281$, with the phase offset $\theta_{ccw} - \theta_m$ approaching $\pi/2$ (Fig. 5). No steady state solution exists for $S > 0.03281$, with intensity pulsations occurring in both the CW and CCW modes.

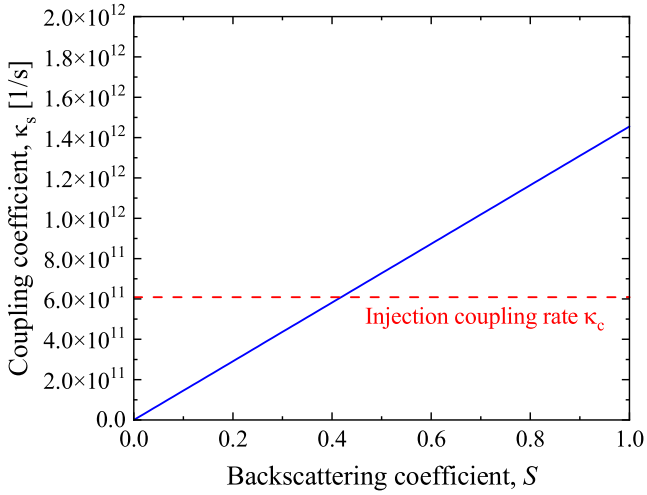

Fig. 4. The coupling coefficient κ_s due to backscattering (blue solid curve) as a function of the amplitude backscattering coefficient S, calculated for the WRL parameters given in Table I. The red dashed line corresponds to the value of injection coupling rate κ_c.

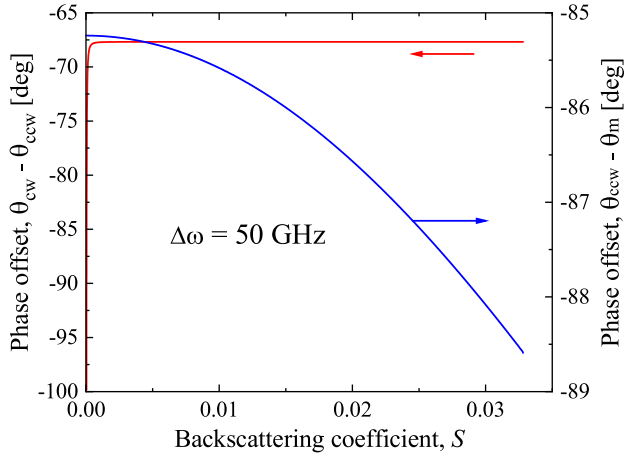

Fig. 5. Optical phase offset between the CW and CCW modes of the injection-locked WRL (red curve) and optical phase offset between the CCW mode and the master laser (blue curve) versus the backscattering coefficient S under steady-state conditions. $I_m = 12$ mA, $I_r = 6$ mA, $\Delta\omega = 50$ GHz.

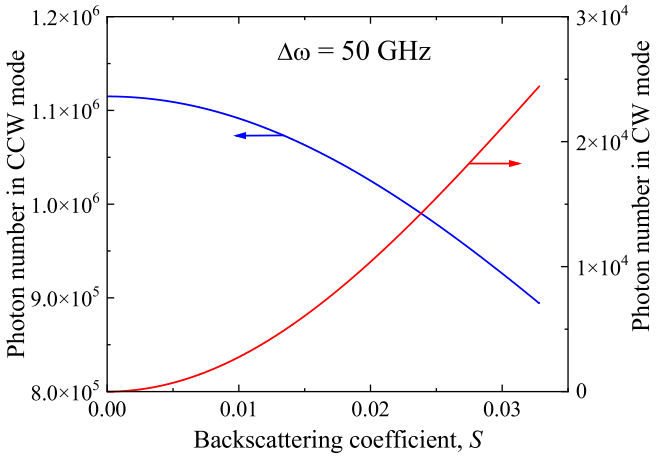

Fig. 6. Photon numbers in the CW and CCW modes of the injection-locked WRL versus the backscattering coefficient S. $I_m = 12$ mA, $I_r = 6$ mA, $\Delta\omega = 50$ GHz.

Figs. 6 and 7 show evolution of the photon number in the CW and CCW modes and of S_{cw}/S_{ccw} intensity ratio, respectively, with increasing values of the backscattering coefficient S. We point out that the total number of photons $S_{cw} + S_{ccw}$ in the ring laser is not conserved. Larger values of S mean more photons from the CCW mode are scattered into the CW mode and lost, thus effectively shortening the photon lifetime for the lasing CCW mode, while the CW mode stays below threshold. The corresponding behavior of the carrier number N_r in the injection-locked WRL is illustrated in Fig. 7. The carrier number increases as the intensity in the lasing CCW mode goes down with enhanced light backscattering.

So far, our analysis has revealed that under relatively strong locking conditions of $\Delta\omega = 50$ GHz the strongly injection-locked WRL would tolerate as much as ~3.28% of light backscattering between the CCW and CW modes, while preserving the injection locking between the master laser and the CCW mode of the WRL.

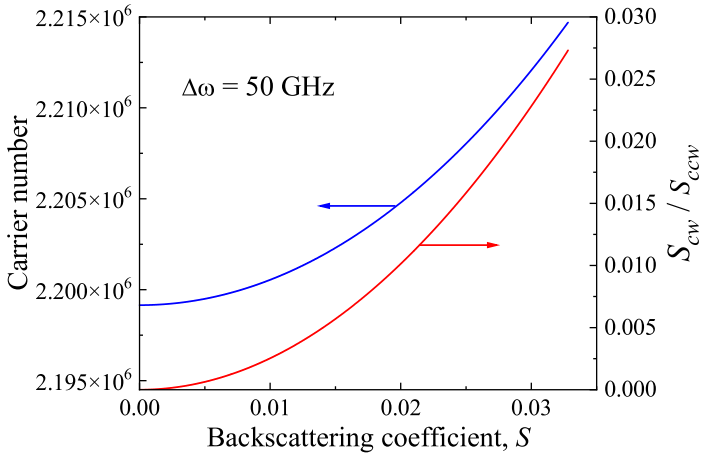

Fig. 7. Intensity ratio for the CW and CCW modes of the injection-locked WRL (red curve) and carrier number in the injection-locked WRL (blue curve) versus the backscattering coefficient S. $I_m = 12$ mA, $I_r = 6$ mA, $\Delta\omega = 50$ GHz.

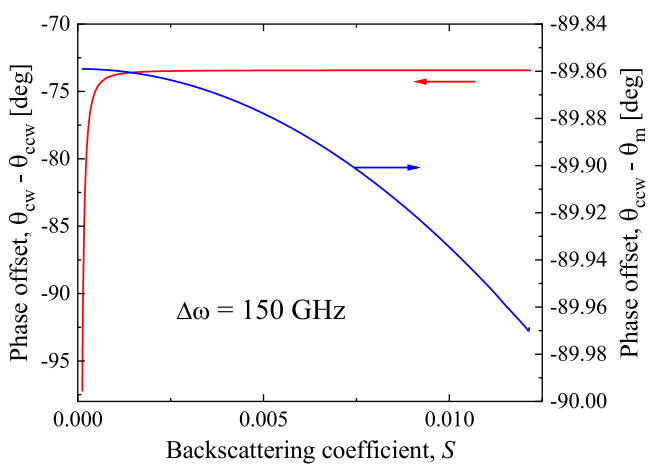

Fig. 8. Optical phase offset between the CCW and CW modes of the injection-locked WRL (red curve) and optical phase offset between the master laser and the CCW mode of the injection-locked WRL (blue curve) versus the backscattering coefficient S under steady-state conditions. $I_m = 12$ mA, $I_r = 6$ mA, $\Delta\omega = 150$ GHz.

The results of similar analysis carried out for the positive frequency detuning $\Delta\omega = 150$ GHz are presented in Figs. 8–10. As follows from Fig. 2, $\Delta\omega = 150$ GHz corresponds to much weaker locking conditions near the boundary of the stable locking range, with much lower intensity circulating in the CCW mode of the WRL. As compared to the case of $\Delta\omega = 50$ GHz, it takes a larger value of the backscattering coefficient $S = 1.21\times10^{-4}$ for the CW mode to get locked by the CCW mode, and a smaller value of $S = 0.01216$ for the injection locking between the master laser and the CCW mode of the WRL to be eventually lost (Fig. 8). Under relatively weak locking conditions of $\Delta\omega = 150$ GHz, therefore, the injection-locked WRL would tolerate ~1.2% of light backscattering between the CCW and CW modes. In Fig. 11, we show the effect of light backscattering on stable locking range attainable in the injection-locked WRL by including the results of similar analysis performed for $\Delta\omega = 80$ GHz and $\Delta\omega = 120$ GHz.

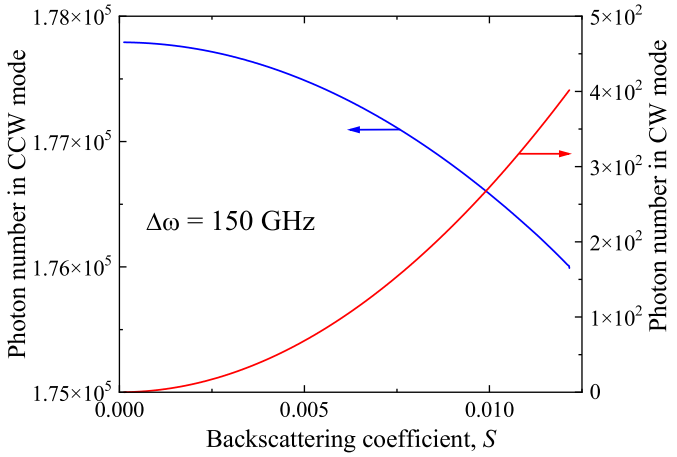

Fig. 9. Photon numbers in the CW and CCW modes of the injection-locked WRL versus the backscattering coefficient S. $I_{\mathrm{m}} = 12$ mA, $I_{\mathrm{r}} = 6$ mA, $\Delta\omega = 150$ GHz.

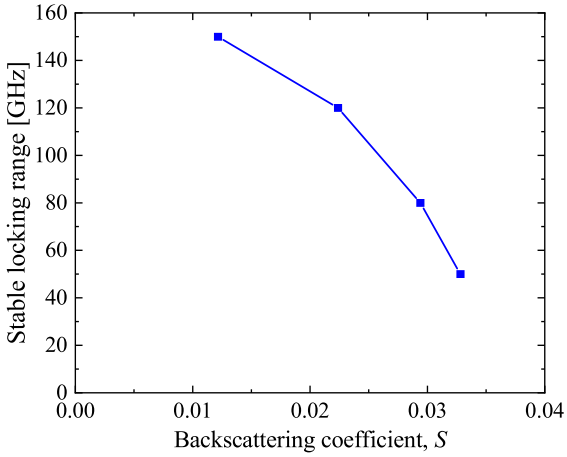

Fig. 11. Stable locking range on the positive frequency detuning side in the injection-locked WRL versus the backscattering coefficient S. $I_{\mathrm{m}} = 12$ mA, $I_{\mathrm{r}} = 6$ mA.

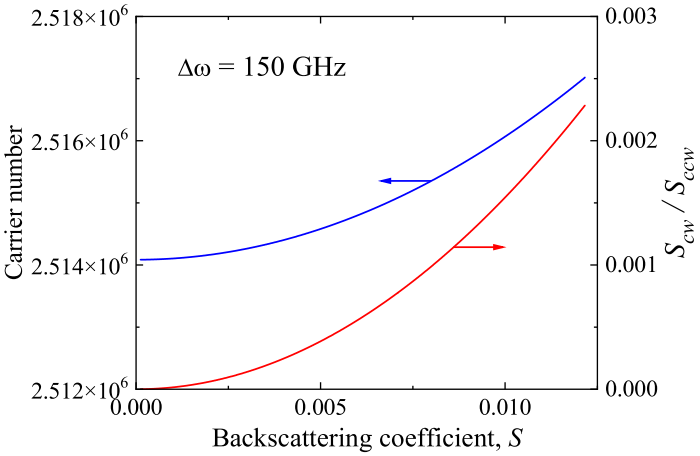

Fig. 10. Intensity ratio for the CW and CCW modes of the injection-locked WRL (red curve) and carrier number in the injection-locked WRL (blue curve) versus the backscattering coefficient S. $I_{\mathrm{m}} = 12$ mA, $I_{\mathrm{r}} = 6$ mA, $\Delta\omega = 150$ GHz.

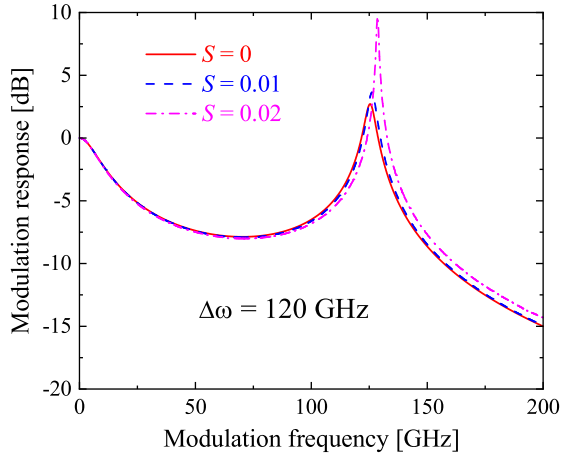

Fig. 12. Modulation frequency response of the injection-locked WRL calculated for several values of the backscattering coefficient S. Modulation frequency response is normalized to its low-frequency value. $I_{\mathrm{m}} = 12$ mA, $I_{\mathrm{r}} = 6$ mA, $\Delta\omega = 120$ GHz.

To calculate the modulation response, a small-signal modulation was applied to the ring laser injection current I_{r} of Eq. (9) in the form

$$I_r = I_{0r}\left[1 + \delta \sin\left(2\pi f t\right)\right], \tag{14}$$

where $I_{0\mathrm{r}}$ is the injection current at a constant ring laser bias, f is the modulation frequency, and δ is the modulation depth. We assumed 1% modulation depth ($\delta = 0.01$) throughout the simulations and present the calculated results in terms of the corresponding modulation depth in the photon number S_{ccw} versus modulation frequency. Fig. 12 shows the modulation response of the WRL calculated for $\Delta\omega = 120$ GHz and several values of the backscattering coefficient S. Increasing the magnitude of S makes the resonance in the modulation response more pronounced. We explain this effect by the frequency detuning $\Delta\omega$ approaching the boundary of the stable locking range that changes with S, as shown in Fig. 11. The effect is similar to the one shown in Fig. 3.

As explained for the first time in [29], there are two components that contribute to enhancement of resonant modulation frequency in injection-locked semiconductor lasers:

$$\omega_{\mathrm{res}} = \Delta\omega_{\mathrm{inj}} - \Delta\omega_{\mathrm{shift}},$$

where $\Delta\omega_{\mathrm{inj}}$ is the frequency detuning between the master laser and the mode of the free-running ring laser and $\Delta\omega_{\mathrm{shift}} = (\alpha/2)a\Delta n\,(\Delta n = n - n_{\mathrm{th}})$ is the carrier-dependent cavity resonance shift. Here n is carrier density, and n_{th} is the threshold carrier density. In the injection-locked laser, carrier density is reduced from its threshold value due to optical injection. The slight shift in the resonance frequency in Fig. 12 is determined by the corresponding change in the second component, $\Delta\omega_{\mathrm{shift}}$, in the expression for ω_{res}. While $\Delta\omega_{\mathrm{inj}}$ remains constant, $\Delta\omega_{\mathrm{shift}}$ decreases with increasing backscattering coefficient S. $\Delta\omega_{\mathrm{inj}}$ effectively approaches the boundary of the stable injection-locking range and carrier density n recovers to its threshold value n_{th}, thus making Δn and $\Delta\omega_{\mathrm{shift}}$ to diminish.

IV. Conclusion

We have previously proposed a strong-injection-locking scheme for enhanced ultra-high-speed performance that involved a single-frequency master laser monolithically integrated with a unidirectional whistle-geometry semiconductor microring laser (WRL) [20], [21]. The WRL scheme is expected to ensure a dramatically increased injection coupling rate due to strong coupling of the master laser output into the ring laser. We confirmed the advantage of this scheme in numerical modeling by predicting greatly enhanced resonance frequency of up to ∼160 GHz for the strongly injection-locked WRL. Our previous analysis, however, did not take into account linear coupling between the two counterpropagating modes due to light backscattering. In this paper, we investigated the possible negative impact of backscattered light on high-speed modulation performance of strongly injection-locked WRLs. We have found out that, depending on frequency detuning between the master laser and the ring laser, the strongly injection-locked WRL tolerates between 1% and 3% of light backscattering between the CCW and CW modes.

References

[1] E. K. Lau, L. J. Wong, and M. C. Wu, "Enhanced modulation characteristics of optical injection-locked lasers: A tutorial," *IEEE J. Sel. Topics Quantum Electron.*, vol. 15, no. 3, pp. 618–633, May–Jun. 2009.

[2] T. B. Simpson, J. M. Liu, and A. Gavrielides, "Bandwidth enhancement and broadband noisereduction in injection-locked semiconductor lasers," *IEEE Photon. Technol. Lett.*, vol. 7, no. 7, pp. 709–711, Jul. 1995.

[3] T. B. Simpson and J. M. Liu, "Enhanced modulation bandwidth in injection-locked semiconductor lasers," *IEEE Photon. Technol. Lett.*, vol. 9, no. 10, pp. 1322–1324, Oct. 1997.

[4] X. M. Jin and S. L. Chuang, "Bandwidth enhancement of Fabry-Perot quantum-well lasers by injection-locking," *Solid-State Electron.*, vol. 50, no. 6, pp. 1141–1149, Jun. 2006.

[5] X. J. Meng, T. Chau, and M. C. Wu, "Experimental demonstration of modulation bandwidth enhancement in distributed feedback lasers with external light injection," *Electron. Lett.*, vol. 34, no. 21, pp. 2031–2032, Oct. 1998.

[6] S. K. Hwang, J. M. Liu, and J. K. White, "35-GHz intrinsic bandwidth for direct modulation in 1.3-μm semiconductor lasers subject to strong injection locking," *IEEE Photon. Technol. Lett.*, vol. 16, no. 4, pp. 972–974, Apr. 2004.

[7] H.-K. Sung et al., "Modulation bandwidth enhancement and nonlinear distortion suppression in directly modulated monolithic injection-locked DFB lasers," in *Proc. MWP Proc. Int. Topical Meeting Microw. Photon.*, 2003, pp. 27–30.

[8] E. K. Lau, X. X. Zhao, H.-K. Sung, D. Parekh, C. Chang-Hasnain, and M. C. Wu, "Strong optical injection-locked semiconductor lasers demonstrating >100-GHz resonance frequencies and 80-GHz intrinsic bandwidths," *Opt. Exp.*, vol. 16, no. 9, pp. 6609–6618, Apr. 2008.

[9] L. Chrostowski, C. H. Chang, and C. J. Chang-Hasnain, "Injection-locked 1.55 μm VCSELs with enhanced spur-free dynamic range," *Electron. Lett.*, vol. 38, no. 17, pp. 965–967, Aug. 2002.

[10] L. Chrostowski, C. H. Chang, and C. J. Chang-Hasnain, "Enhancement of dynamic range in 1.55-μm VCSELs using injection locking," *IEEE Photon. Technol. Lett.*, vol. 15, no. 4, pp. 498–500, Apr. 2003.

[11] Y. Okajima, S. K. Hwang, and J. M. Liu, "Experimental observation of chirp reduction in bandwidth-enhanced semiconductor lasers subject to strong optical injection," *Opt. Commun.*, vol. 219, no. 1–6, pp. 357–364, Apr. 2003.

[12] C. H. Chang, L. Chrostowski, and C. J. Chang-Hasnain, "Injection locking of VCSELs," *IEEE J. Sel. Topics Quantum Electron.*, vol. 9, no. 5, pp. 1386–1393, Sep./Oct. 2003.

[13] X. Zhao et al., "28 GHz optical injection-locked 1.55 μm VCSELs," *Electron. Lett.*, vol. 40, no. 8, pp. 476–478, Apr. 2004.

[14] X. Zhao, L. Chrostowski, and C. J. Chang-Hasnain, "High extinction ratio of injection-locked 1.55-μm VCSELs," *IEEE Photon. Technol. Lett.*, vol. 18, no. 1, pp. 166–168, Jan. 2006.

[15] L. Chrostowski, X. Zhao, C. J. Chang-Hasnain, R. Shau, M. Ortsiefer, and M. Amann, "50-GHz optically injection-locked 1.55-μm VCSELs," *IEEE Photon. Technol. Lett.*, vol. 18, no. 1–4, pp. 367–369, Jan. 2006.

[16] L. Chrostowski, X. Zhao, and C. J. Chang-Hasnain, "Microwave performance of optically injection-locked VCSELs," *IEEE Trans. Microw. Theory Techn.*, vol. 54, no. 2, pp. 788–796, Feb. 2006.

[17] E. Wong, X. Zhao, C. J. Chang-Hasnain, W. Hofmann, and M. C. Amann, "Optically injection-locked 1.55-μm VCSELs as upstream transmitters in WDM-PONs," *IEEE Photon. Technol. Lett.*, vol. 18, no. 22, pp. 2371–2373, Nov. 2006.

[18] L. Chorchos et al., "Energy efficient 850 nm VCSEL based optical transmitter and receiver link capable of 80 Gbit/s NRZ multi-mode fiber data transmission," *J. Lightw. Technol.*, vol. 38, no. 7, pp. 1747–1752, Apr. 2020.

[19] C.-H. Cheng, W.-C. Lo, B. Su, C.-H. Wu, and G.-R. Lin, "Review of VCSELs for complex data-format transmission beyond 100-Gbit/s," *IEEE Photon. J.*, vol. 13, no. 5, Oct. 2021, Art. no. 7900213.

[20] G. A. Smolyakov and M. Osiński, "Rate equation analysis of dynamic response in strongly injection-locked semiconductor microring lasers," *Proc. SPIE*, vol. 7933, 2011, Art. no. 79330D, doi: 10.1117/12.878806.

[21] G. A. Smolyakov and M. Osiński, "High-speed modulation analysis of strongly injection-locked semiconductor ring lasers," *IEEE J. Quantum Electron.*, vol. 47, no. 11, pp. 1463–1471, Nov. 2011.

[22] H. Kalagara, G. A. Smolyakov, and M. Osiński, "Rate equation analysis of *Q*-modulated strongly injection-locked whistle-geometry ring lasers," *IEEE J. Sel. Topics Quantum Electron.*, vol. 21, no. 6, Nov./Dec. 2015, Art. no. 1801909.

[23] L. Chrostowski and W. Shi, "Monolithic injection-locked high-speed semiconductor ring lasers," *J. Lightw. Technol.*, vol. 26, no. 19, pp. 3355–3362, Oct. 2008.

[24] I. V. Ermakov et al., "Semiconductor ring laser with on-chip filtered optical feedback for discrete wavelength tuning," *IEEE J. Quantum Electron.*, vol. 48, no. 2, pp. 129–136, Feb. 2012.

[25] G. Verschaffelt, M. Khoder, and G. Van der Sande, "Optical feedback sensitivity of a semiconductor ring laser with tunable directionality," *Photonics*, vol. 6, no. 4, Dec. 2019, Art. 112.

[26] G. Yuan and S. Yu, "Analysis of dynamic switching behavior of bistable semiconductor ring lasers triggered by resonant optical pulse injection," *IEEE J. Sel. Topics Quantum Electron.*, vol. 13, no. 5, pp. 1227–1234, Sep./Oct. 2007.

[27] Z. Yu and S. Fan, "Integrated nonmagnetic optical isolators based on photonic transitions," *IEEE J. Sel. Topics Quantum Electron.*, vol. 16, no. 2, pp. 459–466, Mar./Apr. 2010.

[28] M. A. Osiński, O. K. Qassim, N. J. Withers, and G. A. Smolyakov, "Light-emitting device having injection-lockable semiconductor ring laser monolithically integrated with master laser," U.S. Pat. 8,009,712, Aug. 30, 2011.

[29] A. Murakami, K. Kawashima, and K. Atsuki, "Cavity resonance shift and bandwidth enhancement in semiconductor lasers with strong light injection," *IEEE J. Quantum Electron.*, vol. 39, no. 10, pp. 1196–1204, Oct. 2003.